Construction of negative electrostatic sugared gourd pore within nickel-based metal-organic framework for one-step purification acetylene from ethylene and carbon dioxide mixture

Guo, X.-Z.; Lin, B.; Xiong, G.-Z.; Krishna, R.; Zhang, Z.-R.; Liu, Q.-Z.; Zhang, Z.-X.; Fan, L.; Zhang, J.; Li, B.

DOI
10.1016/j.cej.2024.154734

Publication date
2024

Document Version
Final published version

Published in
Chemical engineering journal

Chemical Engineering Journal 498 (2024) 154734

Contents lists available at ScienceDirect

Chemical Engineering Journal

journal homepage: www.elsevier.com/locate/cej

Construction of negative electrostatic sugared gourd pore within nickel-based metal-organic framework for one-step purification acetylene from ethylene and carbon dioxide mixture

Xing-Zhe Guo [a,1], Bing Lin [a,1], Guang-Zu Xiong [a,1], Rajamani Krishna [c], Zhao-Rong Zhang [b], Qing-Zan Liu [b], Zhi-Xiong Zhang [b], Liming Fan [d,*], Jie Zhang [b,*], Bingwen Li [a,*]

[a] Shandong Key Laboratory of Biophysics, Institute of Biophysics, College of Chemistry and Chemical Engineering, Dezhou University, Dezhou 253023, PR China
[b] Department of Chemistry and Chemical Engineering, Taiyuan Institute of Technology, Taiyuan 030008, PR China
[c] Van't Hoff Institutefor Molecular Sciences, University of Amsterdam, Science Park 904, 1098 XH Amsterdam, The Netherlands
[d] School of Chemistry and Chemical Engineering, North University of China, Taiyuan 030051, PR China

ARTICLE INFO

Keywords:
Metal-organic frameworks
Sugared gourd pore
One-step purification
Acetylene
Dynamic breakthrough experiment
GCMC simulations

ABSTRACT

The development of highly efficient adsorbents for purifying acetylene from multi-component mixtures is crucial in the chemical industry, yet the tradeoff between renewability and selectivity severely constrains practical industrial applications. This study introduces sugar gourd pore framework (SGPF-1), an innovative ultra-microporous framework synthesized using 1,2-di(4-pyridyl)ethylene (BPE), 4,4′,4″-nitrilotribenzoic acid (NTA), and hexanitronickel under solvothermal conditions. The X-ray diffraction analysis has been used to prove the detailed structure and phase purity of SGPF-1. The structure of SGPF-1 was tailored for selectively adsorbing and separating the target compound, C_2H_2. The negative electrostatic effect, inspired by the natural sugared gourd structure, enhances the selectivity and adsorption capacity for C_2H_2, while minimizing the interaction with impurities like C_2H_4 and CO_2. Experimental data show that SGPF-1 exhibits significantly higher adsorption of C_2H_2 compared to C_2H_4 and CO_2 at 298 K and 100 kPa, demonstrating exceptional selectivity towards 50/50 C_2H_2/CO_2 and 1/99 C_2H_2/C_2H_4 to be 7.33 and 15.46. Breakthrough experiments confirm its effectiveness in separating C_2H_2 from C_2H_4/CO_2 mixtures, with C_2H_4 saturation reached within 5 to 15 min, while C_2H_2 retention time at 298 K was as long as 26 min. Theoretical calculations have revealed that SGPF-1 exhibits electrostatic compatibility with C_2H_2 while repelling C_2H_4 and CO_2 through an electrostatic exclusion mechanism. This highlights the importance of rational pore engineering in optimizing the electrostatic properties of adsorbents for high-efficiency multi-component separations. The research aims to advance gas separation technologies and improve the purity of acetylene, a valuable industrial raw material.

1. Introduction

The natural gas and petrochemical industries are heavily reliant on the efficient and energy-saving separation and purification of light hydrocarbons, particularly ethylene (C_2H_4) and acetylene (C_2H_2) [1,2]. These compounds are crucial precursors for a wide array of products, including chemicals, fibers, plastics, vinyl compounds, rubber, and acrylic acid derivatives [3,4]. The current steam cracking method for producing C_2H_2, however, leads to substantial waste and the emission of greenhouse gases, such as C_2H_4 and carbon dioxide. Moreover, C_2H_2 is detrimental to Ziegler-Natta catalysts during the ethylene polymerization process [5]. It is therefore imperative to develop a technology capable of effectively separating these three gases. Traditional methods, such as low-temperature distillation, are impractical for large-scale operations due to their complex tower designs and the high energy consumption associated with the similar kinetic radii, polarizability, and boiling points of these gases [6,7].

Metal-organic frameworks (MOFs) or porous coordination polymers (PCPs) are a highly promising group of porous materials with diverse compositions, customizable pore structures, and functional pore

* Corresponding authors.
E-mail addresses: limingfan@nuc.edu.cn (L. Fan), zhangjie@tit.edu.cn (J. Zhang), libingwen@dzu.edu.cn (B. Li).
[1] These authors contributed equally.

https://doi.org/10.1016/j.cej.2024.154734
Received 18 May 2024; Received in revised form 6 August 2024; Accepted 9 August 2024
Available online 17 August 2024

surfaces, making them ideal for a wide range of applications, particularly in gas separation [8–16]. Numerous MOFs have been investigated for C_2H_2/C_2H_4 or C_2H_4/CO_2 separations [17]. As a case in point, MOF-74 series, characterized by a high density of open metal sites (OMSs), showcases substantial C_2H_2 storage but tends to exhibit lower selectivity when differentiating between C_2H_2/C_2H_4 and C_2H_4/CO_2 [18–21]. This underscores the need for further investigation into optimizing MOFs structures for improved selectivity in real-world applications (see Scheme 1).

In practical applications, economic feasibility, scalable synthesis, and stability are pivotal factors to consider when evaluating MOFs for single-step C_2H_4 purification [22]. However, many MOFs currently employed in this context face limitations, such as poor stability, high costs, or synthesis scalability, which hinder their widespread industrial adoption. For example, while some C_2H_2/C_2H_6-selective MOFs, like those reported in references [23–25], exhibit superior separation performance, their synthesis often relies on toxic organic solvents, harsh conditions, and expensive, complex organic linkers. These drawbacks translate into elevated production costs and restrict scalability, rendering them unsuitable for large-scale applications. Consequently, it is imperative to identify and develop MOFs that combine outstanding separation efficiency with low cost, high stability and facile scalability to overcome this substantial challenge.

Furthermore, the strategic design of weak interactions, such as electrostatic forces and quadrupole moments, offers a promising alternative to conventional strong chemical adsorption sites, addressing current limitations. These weak interactions facilitate efficient adsorption by exploiting the inherent weak intermolecular forces, allowing for facile desorption. A recent innovation involves exploiting the distinct quadrupole moments of molecules like C_2H_4 ($+6.67 \times 10^{-40}$ cm^2), C_2H_2 ($+20.5 \times 10^{-40}$ cm^2), and CO_2 (-13.4×10^{-40} cm^2), which result in significant variations in adsorption strength when interacting with porous materials. According to electrostatic principles, enhancing the proximity of positive and negative charges intensifies static attraction. Molecular electrostatic potential (MESP) studies reveal that hydrogen atoms in C_2 molecules are uniformly positively charged, with hydrogen atoms in C_2H_2 having a higher charge than in C_2H_4, while oxygen atoms in CO_2 carry a negative charge [26–35]. By leveraging these electrical properties, materials with tailored pore polarizations can be engineered to control the acidity of C_2H_2 or its interaction with CO_2, thereby boosting selective adsorption of these gases. Consequently, the development of MOFs with an electrostatic pore environment holds great potential for single-step purification of C_2H_2 from $C_2H_2/C_2H_4/CO_2$ mixtures, capitalizing on these electrostatic characteristics.

Based on these considerations, ultramicroporous MOFs with specific pore electronegativity are a promising candidates for synthesizing C_2H_2 adsorbents, capable of overcoming the challenges of high capacity storage and high-separation efficiency [6,20]. Thus, a novel sugar gourd pore framework SGPF-1 synthesized using 1,2-di(4-pyridyl)ethylene (BPE), 4,4′,4″-nitrilotribenzoic acid (NTA), and hexanitronickel under

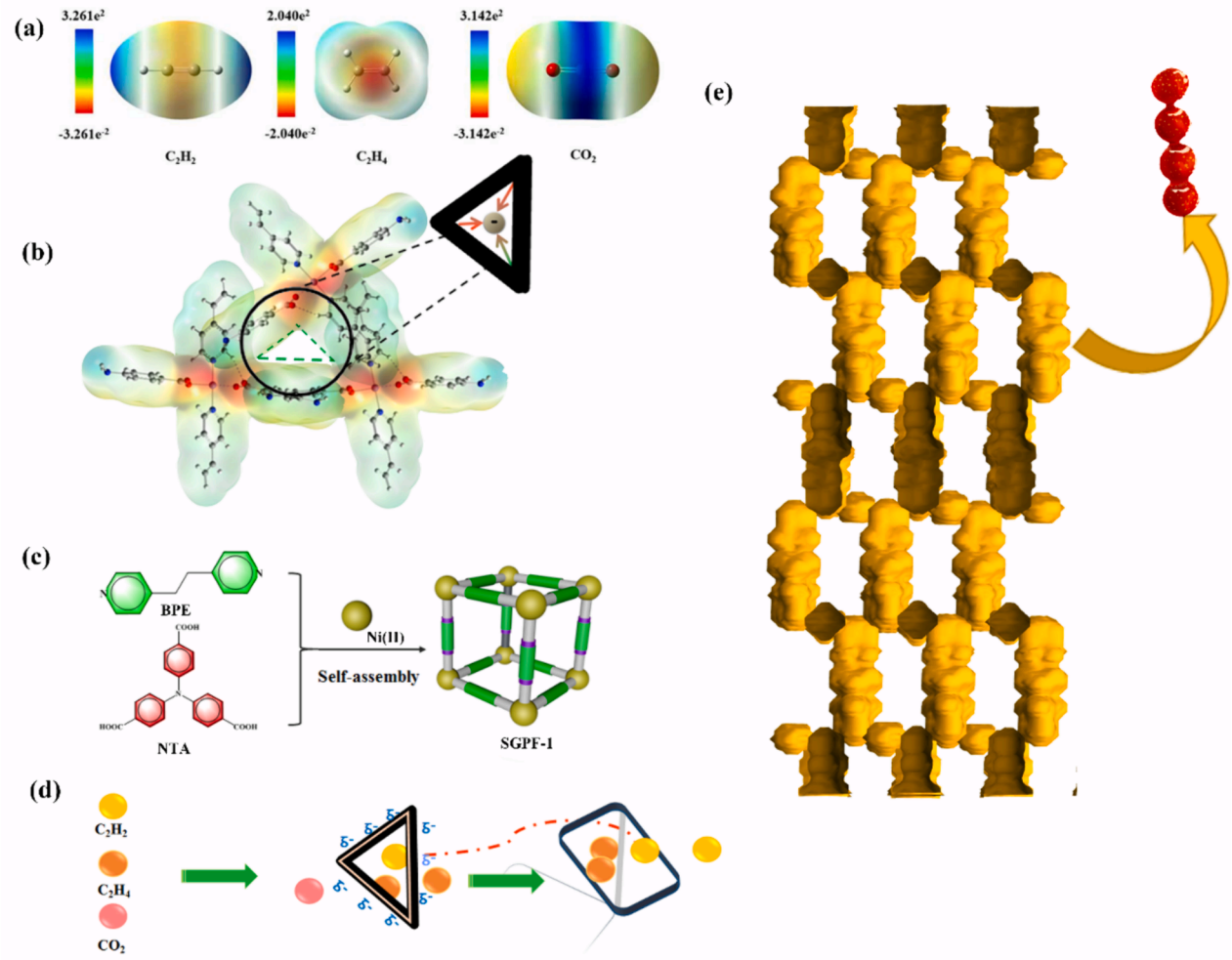

Scheme 1. (a-b) Electrostatic potentials and physiochemical properties of C_2H_2, CH_4, and CO_2. Schematic diagram of pore refinement strategies for SGPF-1 during the self-assembly process. (c) the 3D negative potential triangular pore in SGPF-1. (d) the detailed adsorption separation process of SGPF-1 for the mixture of C_2H_2/CH_4/CO_2. (e) the sugar gourd pore of SGPE-1.

solvothermal conditions, features an acetylene-affinity channel for efficient C_2H_2 capture. This strategy has been demonstrated in the supermicroporous MOFs with two different pore structures: one with negatively charged triangular cavities, achieving effective separation of C_2 molecules and CO_2; the other pore was cut upon introduction of the second ligand to achieve efficient separation of C_2H_2 and C_2H_4. The result has proved that SGPF-1 exhibits exceptionally high C_2H_2 uptake than that of C_2H_4 and CO_2. Notely, in the ternary mixture $C_2H_2/CO_2/C_2H_4$ (25/50/25, v/v/v), C_2H_4 displayed rapid and pure elution within the first five minutes, CO_2 eluted after approximately 15 min, while C_2H_2 exhibited prolonged retention, being effectively trapped in the material until saturation was reached. DFT calculations reveal that the H/O sites on the channel pore surface exhibit stronger multiple interactions with C_2H_2 compared to C_2H_4 and CO_2. Experimental breakthrough tests confirm that C_2H_2 (99.9 % purity) can be selectively separated from a ternary C2 mixture, achieving the highest yield of 0.74 mmol/g. SGPF-1 holds significant potential for achieving high stability, low cost, and scalable efficient separation.

2. Experimental

2.1. Synthesis of SGPF-1

A synthesis protocol was developed by combining DMF (2 ml), H_2O (2 ml), and a single drop of a 6 M DMF solution of nickel nitrate hexahydrate. The mixture was fortified with 15 mg each of NTA and BPE and heated at a constant temperature of 100 °C for three days, which led to the formation of a green precipitate. To ensure the purity of the product, the green powder was washed thrice with ethanol. Following purification, the sample was subjected to dehydration in a vacuum oven at 100 °C for 12 h before proceeding to further experiments.

3. Results and discussion

3.1. Structure description

Single-crystal X-ray analysis reveals that SGPF-1 crystallizes in the orthorhombic space group P1 (Supporting Information, Tables S1-S2). The asymmetric unit of SGPF-1 is composed of a single crystalline Ni atom, a BPE ligand, an NTA ligand, and two lattice water molecules functioning as solvent molecules (Fig. S1a). At its central core, Ni1 forms a mononuclear {NiO2N2} second building units (SBU), coordinating with unique N atoms from the separate pyridine groups of the two BPE ligands, O atoms from the carboxylate groups of the NTA ligand and two water molecules. It is worth highlighting that the carboxylate group in SGPF-1 was partially deprotonated, which contributes to the emergence of open metal sites (OMS) during the self-assembly process. The Ni-N interaction gives rise to a linear one-dimensional arrangement, while Ni-O interactions form a two-dimensional framework (Supporting Information, Fig. S1-2). The interconnected Ni sites, coupled with the extended BPE and NTA chains, collectively contribute to a 3D structure showcasing dual microporosity along the c and b axis. (Fig. 1b-c). Analysis of the SGPF-1 channels along the b axis highlights the distinct features akin to a sugar gourd with a notable porosity of 20.8 % (Fig. 1d).

In the topological analysis, designating NTA ligands and mononuclear units as 3 and 4 connect, respectively, the structure of SGPF-1 can be symbolically represented as a 2-node 3D framework with the point symbol of $\{10^3\}_2\{10^6\}_3$ (Fig. 1e). These ultramicroporous structural features can help improve the adsorption and separation performance of SGPF-1 for C_2H_2. In addition, the uncoordinated carboxylate O (O4I, O4H and O4G) can form a 3D triangular pore (6.467, 6.467, 6.467) during the assembly process, which serves as Lewis basic binding sites that provide strong binding affinity to C_2H_2 through hydrogen bonding and provide a perfect confined space and MESP for selective capture of C_2 molecules from C_2 molecules/CO_2 mixtures (Fig. 1f). In addition,

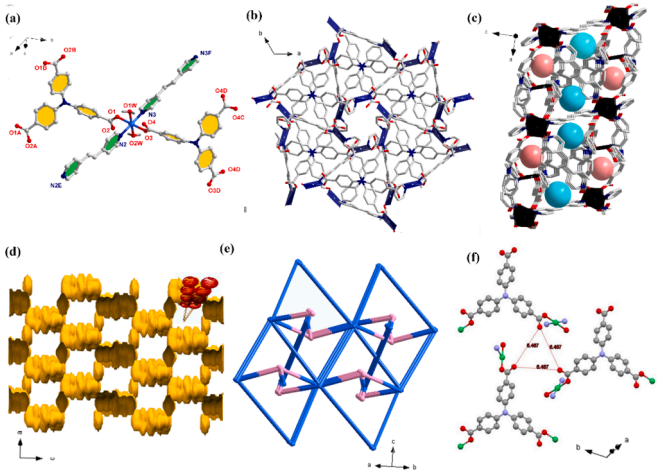

Fig. 1. (a) The asymmetric unit of SGPF-1. (b-c) the 3D framework structure of SGPF-1. (d) the visualized pore structure of SGPF-1. (e) the topology of SGPF-1. (f) the negative potential triangle 3D pore.

other types of 1D microporous structures had appropriate pore size to prevent the entry of C_2H_4, which enabled effective separation of C_2H_2/C_2H_4 to a certain extent. The triangular structure, along with Lewis basic sites and OMS, could serve as an ideal capsule for C_2H_2, potentially leading to the top-level separation of C_2H_2/CO_2 and further increasing the storage capacity of C_2H_2. These promising structural features lead us to evaluate the C_2H_2 storage and C_2H_2/CO_2 separation performance of SGPF-1.

3.2. X-ray power diffraction analyses and thermal analyses

The crystal structure of SGPF-1 is illustrated in Fig. S2-4 by powder X-ray diffraction (PXRD) patterns and thermogravimetric analysis (TGA). It can be seen that the PXRD patterns of samples exhibit distinctive diffraction peaks ($2\theta = 8.7$, 13.3, 14.2, 17.4, 19.9, 20.7, 21.6, and 21.8°), which closely match the outcomes of the simulations (Fig. S2). TGA was performed to evaluate the thermal stability of SGPF-1. It was shown that SGPF-1 can be stable up to 380 °C (Fig. S3). The study systematically investigated the stability of SGPF-1 by exposing it to a variety of solvents (water, ethanol, and methanol) and diverse pH conditions in order to examine alterations in their PXRD patterns. The unambiguous experimental outcomes demonstrated that the core peak positions within the PXRD patterns of SGPF-1 remained constant across all tested conditions, reinforcing the exceptional stability of these materials. The structural stability of SGPF-1 has been further confirmed by immersing the samples in various solvents and analyzing them with FT-IR and TGA (Fig. S3). Furthermore, PXRD patterns of SGPF-1 were collected at temperatures ranging from 40 °C to 200 °C, providing compelling evidence for the thermal stability of materials. Additional data was obtained through the analysis of PXRD patterns at temperatures ranging from 40 °C to 200 °C, providing supplementary evidence for the thermal stability of SGPF-1 (Fig. S4).

3.3. Performance characterization

3.3.1. Single-component gas isotherms and separation performance

To assess the porosity of SGPF-1, we initially conducted measurements of their static volumetric pure-gas isotherms, which provide insights into the adsorption capacity of a given sorbent. However, SGPF-1 exhibited a low N_2 uptake of 14.3 cm^3/g at 77 K (Fig. 2). Conversely, CO_2 adsorption isotherms at 195 K have verified the permanent porosity of SGPF-1 by demonstrating the distinctive type-I adsorption behavior typical of microporous materials (Fig. 2a). The adsorption capacity of SGPF-1 was determined to be 102.7 cm^3/g. Moreover, the permanent

porosity of SGPF-1 was determined from CO_2 adsorption isotherms at 195 K, revealing a Brunauer – Emmett – Teller (BET) surface area of 361.04 m^2/g, which closely aligns with the theoretical BET value of 370.79 m^2/g (Fig. S5). In addition, the DFT method estimates that the pore size distributions peak at 3.5 and 5.2 Å, demonstrating excellent agreement with the calculated values derived from the crystal structures.

Considering the stability of the pore channels, the Grand canonical Monte Carlo (GCMC) simulations were employed to calculate the adsorption capacities of SGPF-1 for single-component gases at 298 K (Fig. 2b). Based on the experimental findings, it can be inferred that the simulated adsorption capacities of SGPF-1 for C_2H_2, CO_2, and C_2H_4 are 1.89 mmol/g, 1.27 mmol/g, and 1.04 mmol/g, respectively. Evidently, in comparison to the other two gases, SGPF-1 demonstrates superior adsorption performance towards C_2H_2. To test this hypothesis, C_2H_2, CO_2 and C_2H_4 adsorption experiments were conducted at 273 K and 298 K (Fig. 2c-d), respectively. As shown in Fig. 2d SGPF-1 exhibit higher C_2H_2 uptake (1.92 mmol/g) than CO_2 (1.27 mmol/g), and C_2H_4 (0.75 mmol/g) at 298 K and 100 kPa, respectively. Significantly, the C_2H_2 adsorption isotherm of SGPF-1 is much steeper than that of C_2H_4 and CO_2 in the low-pressure region (Fig. 2e-f). The sequence of affinity between the framework and guest molecules is $C_2H_2 > C_2H_4 > CO_2$. So that trace gases can be separated even at low partial pressures, steep adsorption isotherms are necessary.

The selectivity of C_2H_2/CO_2 and C_2H_2/C_2H_4 on SGPF-1 was determined using ideal adsorbed solution theory (IAST) after fitting the isotherms to the dual site Langmuir equation. The IAST selectivity for 50/50 C_2H_2/CO_2, 50/50 of CO_2/C_2H_4 and 1/99 of C_2H_2/C_2H_4 are 7.33, 1.99 and 15.46 in SGPF-1, respectively (Fig. 2g-i). These exceptional selectivities surpass those of numerous reference materials (Table S4) [36–50], demonstrating the superior performance of SGPF-1 in selectively adsorbing these gases (Fig. 2j). The isosteric enthalpy of adsorption (Q_{st}) plys a pivotal role in assessing the separation efficiency of materials, with higher values indicating a stronger adsorbate-material interaction, which in turn increases regeneration energy consumption (Fig. 2k). Consequently, moderately elevated Q_{st} values are preferred. To evaluate the performance of SGPF-1, single-component isotherms for C_2H_2, CO_2, and C_2H_4 at 273 and 298 K were obtained utilizing the Clausius-Clapeyron equation. Notably, the Q_{st} value for C_2H_2 at near-zero loading was found to be 56.7 kJ/mol, significantly higher than that of C_2H_4 (40.0 kJ/mol) and CO_2 (32.6 kJ/mol), indicating the strong affinity of SGPF-1 for C_2H_2. In addition, the separation potential (Δq) served as a comprehensive indicator to assess both selectivity and capacity. These findings demonstrate that Δq values of SGPF-1 for C_2H_2/CO_2 (v/v = 50/50), C_2H_2/C_2H_4 (v/v = 1/99), CO_2/C_2H_4 (v/v = 50/50) and $C_2H_2/C_2H_4/CO_2$ (v/v/v = 25/50/25) are 1.35, 10.5, 0.36 and 1.3 mol kg^{-1}, respectively, which substantiate the efficacy of SGPF-1 in purifying C_2H_4 from a mixture of C_2H_2 and CO_2 (Fig. 2l and Fig. S6-7).

3.3.2. *Dynamic column breakthrough studies*

Dynamic breakthrough experiments were conducted to verify effectiveness of SGPF-1 in separating different mixture proportions. A stainless column with dimensions of Φ 4.6 mm × 50 mm was filled with 550 mg of SGPF-1 powder for the experiments. The feasibility of separating products in a packed column using SGPF-1 was verified by employing the method described by Krishna to conduct transient breakthrough simulations on C_2H_2/CO_2 (50/50, v/v), C_2H_2/C_2H_4 (1/99, v/v), and C_2H_4/CO_2 (50/50, v/v) mixtures under the conditions of 298 K and 100 kPa After activating the sample by Ar purge at 70 ∘C for 12 h (Fig. 3a–c).

For binary C_2H_2/C_2H_4 mixtures (1/99, v/v) with a flow rate of 2 mL min^{-1}, C_2H_4 rapidly passed through the SGPF-1 at 298 K, while C_2H_2

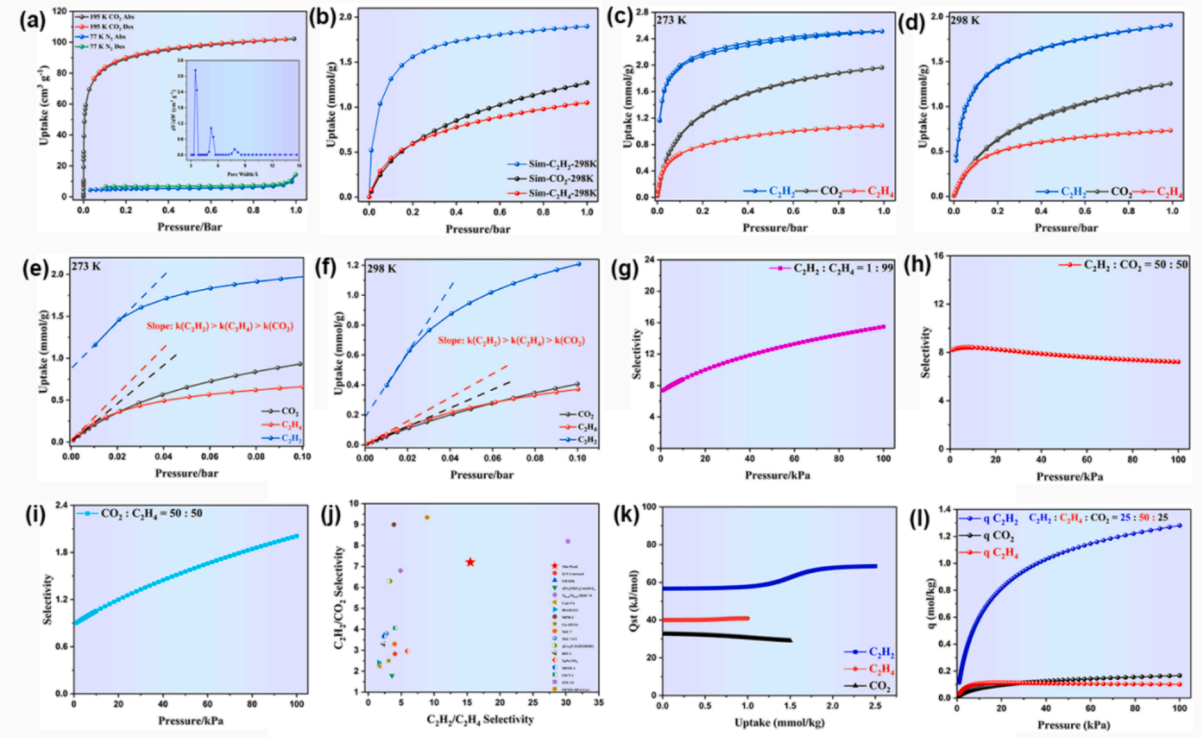

Fig. 2. (a) CO_2 sorption isotherms for SGPF-1. (b) The simulation of C_2H_2, CO_2, and C_2H_4 adsorption isotherms of SGPF-1. (c) Adsorption isotherms for C_2H_2, CO_2, and C_2H_4 on SGPF-1 at 273 K; (d) Adsorption isotherms for C_2H_2, CO_2, and C_2H_4 on SGPF-1 at 298 K. (e) The slope of the adsorption isotherms of C_2H_2, CO_2, and C_2H_4 on SGPF-1 at 273 K. (f) The slope of the adsorption isotherms of C_2H_2, CO_2, and C_2H_4 on SGPF-1 at 273 K 298 K. (g) IAST calculations of SGPF-1 for mixtures of C_2H_2/C_2H_4 (1/99). (h) IAST calculations of SGPF-1 for mixtures of C_2H_2/CO_2 (50/50). (i) IAST calculations of SGPF-1 for mixtures of CO_2/C_2H_4 (50/50); (j) The Qst value of SGPF-1 at 298 K. (k) A comparison between the IAST selectivity C_2H_2/C_2H_4 of SGPF-1 with other MOFs. (l) The separation potential of SGPF-1 for the mixture of $C_2H_2/C_2H_4/CO_2$ (v/v/v = 25/50/25).

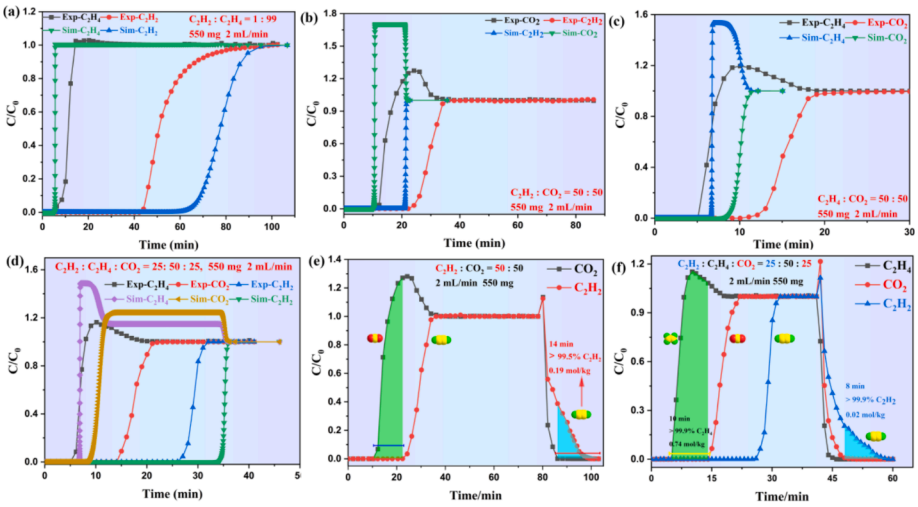

Fig. 3. Simulated and experimental breakthrough curves of SGPF-1 for: (a) C_2H_2/CO_2 mixtures 50/50; (b) C_2H_2/C_2H_4 mixtures 1/99. (c) C_2H_4/CO_2 mixtures 50/50. (d) $C_2H_2/C_2H_4/CO_2$ mixtures 25/50/25. (e) the separation and desperation of C_2H_2/CO_2 mixtures 50/50 and (f) $C_2H_2/C_2H_4/CO_2$ mixtures 25/50/25.

exhibited a retention time of 57.5 min (Fig. 3a). For C_2H_2/CO_2 mixtures (50:50, v/v), CO_2 rapidly permeated at 9.6 min, whereas C_2H_2 was retained until 22 min under the same conditions (Fig. 3b). For C_2H_4/CO_2 mixtures (50:50, v/v), C_2H_4 rapidly permeated at 6.3 min, whereas CO_2 was retained until 6.5 min under the same conditions (Fig. 3c). Based on the simulation results, breakthrough experiments were conducted at 298 K. The detailed elution times are shown in Table S5, demonstrating consistent elution times between experiment and simulation, thus reinforcing the superior gas separation performance of the material. To further evaluate the multicomponent separation capabilities of SGPF-1, transient breakthrough experiments were performed on a ternary mixture $C_2H_2/CO_2/C_2H_4$ (25/50/25, v/v/v) at 8 mL min^{-1} and 298 K, 100 kPa. The experimental results showed that C_2H_4 was the first component to be eluted with high purity. After approximately 15 min, CO_2 started to be eluted, while C_2H_2 remained trapped in the material until saturation (Fig. 3d). This indicates that SGPF-1 has the capability to selectively separate and retain different components of the mixture. After achieving a complete breakthrough, the separation C_2H_2/CO_2 and $C_2H_2/C_2H_4/CO_2$ gases was desperation using Ar gas at a flow rate of 10 mL min^{-1} for material regeneration. It is noteworthy that at 70 °C, nearly all of the C_2H_2/CO_2 gas is desorption within 24 min, while the desorption of $C_2H_2/C_2H_4/CO_2$ gas takes only 20 min, allowing for further use of the material (Fig. 3e-3f). Furthermore, the cycle breakthrough tests were carried out under identical conditions, and the findings demonstrated that SGPF-1′s breakthrough performance did not exhibit a significant decrease over three cycles. This suggests that the material exhibits favorable recyclability in separating $C_2H_2/CO_2/C_2H_4$ (Fig. S8).

3.3.3. *Molecular simulations*

The molecular-level adsorption behavior of C_2H_2, C_2H_4, and CO_2 on SGPF-1 was systematically investigated using the Large Gauge Monte Carlo (GCMC) method. A strong interaction between C_2H_2 and the SGPF-1 framework was observed, primarily through C—O···H van hydrogen bonds interactions and multiple C—H···H van der Waals interactions, with binding distances ranging from 2.53 to 3.93 Å (Fig. 4a). This indicates close binding of C_2H_2 to carboxyl O or N sites on the triangular channel surface (Fig. 4b). C_2H_4 exhibited hydrogen bonding, albeit at slightly shorter distances (2.51–3.35 Å), while CO_2 had a longer range (3.03–4.02 Å) due to C—O···H and C—O···C bonds (Fig. 4c). The study highlights the significant influence of pore size and electrostatic properties for SGPF-1 on its adsorption capabilities. At 298 K 100 kPa, C_2H_2 had a higher distribution density compared to C_2H_4 and CO_2, with adsorption capacities of 47.0 mmol/g, 31.5 mmol/g, and 26.0 mmol/g, respectively (Fig. 5). These findings are in line with the experimental adsorption characteristics, highlighting the triangle-like pores and high density of unprotonated O and H sites in SGPF-1, which contribute to its superior selectivity for C_2H_2 over CO_2 and C_2H_4. Consistent with the heat of adsorption (Q_{st}) calculated from one-component gas adsorption isotherms, this research emphasizes the material's potential for efficient multi-component gas separation, particularly in C_2H_2 adsorption. In conclusion, the study provides valuable insights for designing and optimizing adsorption materials tailored for enhanced multi-component gas separation.

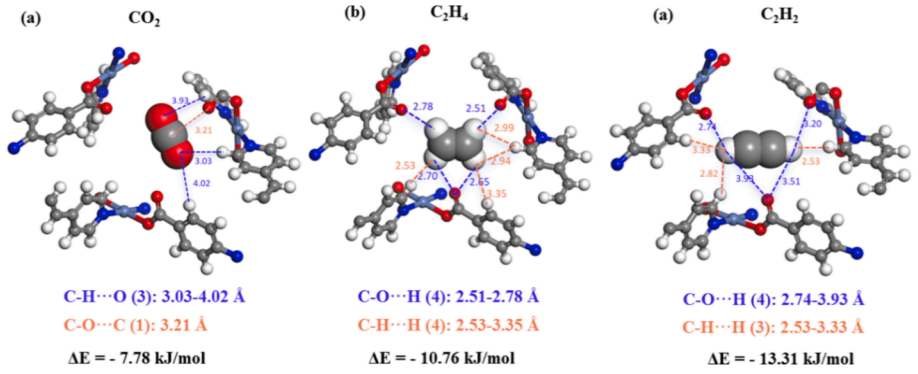

Fig. 4. The adsorption binding sites of (a) CO_2@ SGPF-1, (b) C_2H_4@ SGPF-1, (c) C_2H_2@ SGPF-1 calculated by DFT.

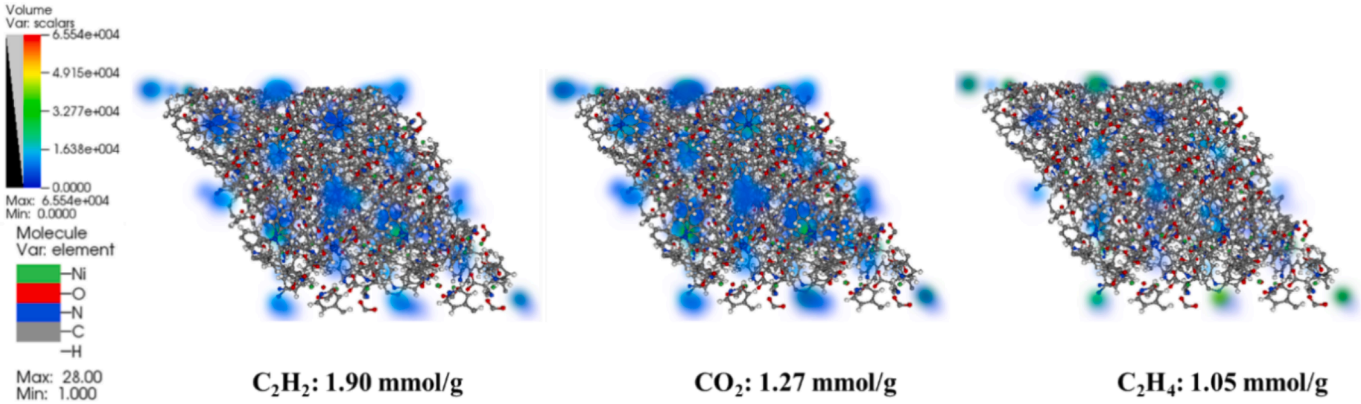

Fig. 5. The GCMC simulation of density distribution of C_2H_2, CO_2 and C_2H_4 within the pore of SGPF-1 at 298 K and 100 kPa.

4. Conclusion

In conclusion, the dual ligands strategy has been employed for the successfully synthesis of SGPF-1, exhibiting enhanced stability and superior gas adsorption capabilities. The material's improved thermal/chemical stability, optimal pore size, and high skeletal density can be attributed to the partial deprotonation of carboxylate acid ligands (NTA) and the incorporation of a second nitrogen-based ligands (BPE). SGPF-1 boasts two distinct ultramicroporous structures: a negatively charged triangular cavity facilitating effective C_2/CO_2 separation, and a cubic structure with pores strategically modified upon the introduction of the second ligand for efficient C_2H_2/C_2H_4 discrimination. This work highlights significant advancements in tackling challenges related to acetylene storage and multicomponent separation, particularly in C_2H_2/CO_2 and C_2H_2/C_2H_4 mixtures, with notable purification performance demonstrated in dynamic breakthrough experiments. GCMC simulations underscore the role of compatible pore environments and weak electrostatic interactions in driving efficient C_2H_2 separation. Consequently, this research prompts the development of charged pore adsorbents to overcome the inherent trade-off between reproducibility and selectivity, thereby addressing the complexities of multicomponent system separation in the chemical industry.

5. The authorship contribution statement

Xing-Zhe Guo was responsible for the conceptualization and direction of the project. Bing Lin and Guang-Zu Xiong were involved in designing the detector. Rajamani Krishna conducted index analysis of adsorption separation. Zhao-Rong Zhang, Qing-Zan Liu, and Zhi-Xiong Zhang oversaw compound synthesis, purification, and characterization. Liming Fan and Jie Zhang contributed to writing and editing the manuscript. Bingwen Li provided computational support. All authors offered valuable feedback and approved the final version of the manuscript.

CRediT authorship contribution statement

Xing-Zhe Guo: Conceptualization. **Bing Lin:** Data curation. **Guang-Zu Xiong:** Data curation. **Rajamani Krishna:** Methodology. **Zhao-Rong Zhang:** Investigation. **Qing-Zan Liu:** Investigation. **Zhi-Xiong Zhang:** Investigation. **Liming Fan:** Writing – review & editing. **Jie Zhang:** Writing – review & editing, Conceptualization. **Bingwen Li:** Methodology.

Declaration of competing interest

The authors declare that they have no known competing financial interests or personal relationships that could have appeared to influence the work reported in this paper.

Data availability

The authors do not have permission to share data.

Acknowledgment

The acknowledgements come at the end of an article after the conclusions and before the notes and references. Natural Science Foundation of Shandong Province (ZR2021QB159). This work is also supported by the Talent Program Foundation of Dezhou University (NO. 2021xjrc102), the authors acknowledge financial assistance from the Natural Science Foundation of Shanxi Province (No. 202203021211090), the National Natural Science Foundation of China (No. 21801230), and the Young Academic Leader Supported Program of North University of China (No. QX201904). The Natural Science Foundation of Shanxi Province (202203021212331), Science and Technology Innovation Project of Colleges and Universities of Shanxi Province (2022L532). The Youth Innovation Team Lead-education Project of Shandong Educational Committee. CCDC number 2349983.

Appendix A. Supplementary material

Supplementary data to this article can be found online at https://doi.org/10.1016/j.cej.2024.154734.

References

[1] Y. Chai, X. Han, W. Li, S. Liu, S. Yao, C. Wang, W. Shi, I. da-Silva, P. Manuel, Y. Cheng, L. D. Daemen, A. J. Ramirez-Cuesta, C. C. Tang, L. Jiang, S. Yang, N. Guan, L. Li, Control of zeolite pore interior for chemoselective alkyne/olefin separations, Science 368 (6494) (2020) 1002–1006.
[2] H. Wang, Y. Liu, J. Li, Designer metal–organic frameworks for size-exclusion-based hydrocarbon separations: progress and challenges, Adv. Mater. 32 (44) (2020).
[3] T. Ren, M. Patel, K. Blok, Olefins from conventional and heavy feedstocks: Energy use in steam cracking and alternative processes, Energy 31 (4) (2006) 425–451.
[4] Y.L. Peng, T. Pham, P. Li, T. Wang, Y. Chen, K.J. Chen, K.A. Forrest, B. Space, P. Cheng, M.J. Zaworotko, Z. Zhang, Robust ultramicroporous metal–organic frameworks with benchmark affinity for acetylene, Angew. Chem. Int. Ed. 57 (34) (2018) 10971–10975.
[5] Z. Jiang, W. Wang, W. Xue, H. Zhu, H. Huang, C. Zhong, Construction of π back donation active site in metal-organic framework for dense packing of C2H2 and efficient C_2H_2/CO_2 separation, Sep. Purif. Technol. 322 (2023) 124345.
[6] O.T. Qazvini, L.K. Macreadie, S.G. Telfer, Effect of ligand functionalization on the separation of small hydrocarbons and CO_2 by a series of MUF-15 analogues, Chem. Mater. 32 (15) (2020) 6744–6752.
[7] O.T. Qazvini, R. Babarao, Z.-L. Shi, Y.-B. Zhang, S.G. Telfer, A robust ethane-trapping metal–organic framework with a high capacity for ethylene purification, J. Am. Chem. Soc. 141 (12) (2019) 5014–5020.
[8] X.-Z. Guo, B. Li, G.-Z. Xiong, B. Lin, L.-C. Gui, X.-X. Zhang, Z. Qiu, R. Krishna, X. Wang, X. Yan, S.-S. Chen, A stable ultramicroporous Cd (II)-MOF with accessible oxygen sites for efficient separation of light hydrocarbons with high methane production, Sep. Purif. Technol. 334 (2024) 125987.

[9] X. Han, C. Zhao, S. Wang, Z. Pan, Z. Jiang, X. Tang, Multifunctional TiO_2/C nanosheets derived from 3D metal–organic frameworks for mild-temperature-photothermal-sonodynamic-chemodynamic therapy under photoacoustic image guidance, J. Colloid Interface Sci. 621 (2022) 360–373.

[10] S. Zhang, R. Shi, K. Cai, T. Wang, T. Qu, L. Li, X. Lang, Coordination networks in accordion-like copper based metal–organic frameworks facilitate efficient catalytic strategies in high performance lithium-sulfur batteries, J. Electroanal. Chem 967 (2024) 118468.

[11] C. Zhao, X. Tang, X. Chen, Z. Jiang, Multifaceted carbonized metal–organic frameworks synergize with immune checkpoint inhibitors for precision and augmented cuproptosis cancer therapy, ACS Nano 18 (27) (2024) 17852–17868.

[12] C. Zhao, X. Tang, J. Zhao, J. Cao, Z. Jiang, J. Qin, MOF derived core-shell CuO/C with temperature-controlled oxygen-vacancy for real time analysis of glucose, J. Nanobiotechnology 20 (1) (2022) 507.

[13] D. Guo, H. Li, Y. Zhang, Y. Nie, X. Feng, Y. Wu, X. Zhao, Z. Xu, Y. Wang, A multifunctional MOF-on-MOF-based dual-channel luminescent signal readout strategy for classifying phenylglyoxylic acid and 2, 6-dipicolinic acid, Cryst. Growth Des. 24 (12) (2024) 5251–5262.

[14] X. Long, K. Chong, Y. Su, C. Chang, L. Zhao, Meso-scale low-cycle fatigue damage of polycrystalline nickel-based alloy by crystal plasticity finite element method, Int J. Fatigue 175 (2023) 107778.

[15] X. Long, Z. Shen, J. Li, R. Dong, M. Liu, Y. Su, C. Chen, Size effect of nickel-based single crystal superalloy revealed by nanoindentation with low strain rates, J. Mater. Res. Technol. 29 (2024) 2437–2447.

[16] J. Qun, C. Xu, X. Xu, Y. Zhao, Y. Zhao, Y. Zhao, J. Wang, Porous covalent organic framework based hydrogen-bond nanotrap for the precise recognition and separation of gold, Angew. Chem. Int. Ed. 135 (17) (2023) e202300459.

[17] X. Jiang, T. Pham, J.-W. Cao, K.A. Forrest, H. Wang, J. Chen, Q.-Y. Zhang, K.-J. Chen, Molecular sieving of acetylene from ethylene in a rigid ultra-microporous metal organic framework, Chem. Eur. J. 27 (2021) 9446.

[18] R. Yang, Y. Wang, J.-W. Cao, Z.-M. Ye, P. Tony, K.A. Forrest, K. Rajamani, H. Chen, L. Li, B.-K. Ling, T. Zhang, T. Gao, X. Jiang, X.-O. Xu, Q.-H. Ye, K.-J. Chen, Hydrogen bond unlocking-driven pore structure control for shifting multi-component gas separation function, Nat Commun 15 (1) (2024) 804.

[19] G. Ding, C. Li, L. Chen, G. Liao, Emerging porphyrin-based metal-organic frameworks for photo (electro) catalytic CO_2 reduction. Energy Environ. Sci., 2024, Advance Article.

[20] J. Zhang, X. Guo, B. Lin, G. Xiong, H. Wang, M. Zhang, L. Fan, B. Li, S. Chen, Efficient adsorption separation of methane from C2–C3 hydrocarbons in a Co(II)-nodes metal–organic framework, Chinese J. Chem. Eng. 69 (2024) 192–198.

[21] M.L. Foo, R. Matsuda, Y. Hijikata, R. Krishna, H. Sato, S. Horike, A. Hori, J. Duan, Y. Sato, Y. Kubota, M. Takata, S. Kitagawa, An adsorbate discriminatory gate effect in a flexible porous coordination polymer for selective adsorption of CO_2 over C_2H_2, J. Am. Chem. Soc. 138 (9) (2016) 3022–3030.

[22] J. Pei, H.-M. Wen, X.-W. Gu, Q.-L. Qian, Y. Yang, Y. Cui, B. Li, B. Chen, G. Qian, Dense packing of acetylene in a stable and low-cost metal–organic framework for efficient C_2H_2/CO_2 separation, Angew. Chem. Int. Ed. 60 (47) (2021) 25068–25074.

[23] H.-G. Hao, Y.-F. Zhao, D.-M. Chen, J.-M. Yu, K. Tan, S. Ma, Y. Chabal, Z.-M. Zhang, J.-M. Dou, Z.-H. Xiao, G. Day, H.-C. Zhou, T.-B. Lu, Simultaneous trapping of C_2H_2 and C_2H_6 from a ternary mixture of $C_2H_2/C_2H_4/C_2H_6$ in a robust metal–organic framework for the purification of C_2H_4, Angew. Chem. Int. Ed. 130 (49) (2018) 16299–16303.

[24] B. Zhu, J.-W. Cao, S. Mukherjee, T. Pham, T. Zhang, T. Wang, X. Jiang, K. A. Forrest, M.J. Zaworotko, K.-J. Chen, Pore engineering for one-step ethylene purification from a three-component hydrocarbon mixture, J. Am. Chem. Soc. 143 (3) (2021) 1485–1492.

[25] P. Zhang, Y. Zhong, Y. Zhang, Z. Zhu, Y. Liu, Y. Su, J. Chen, S. Chen, Z. Zeng, H. Xing, S. Deng, J. Wang, Synergistic binding sites in a hybrid ultramicroporous material for one-step ethylene purification from ternary C_2 hydrocarbon mixtures, Sci. Adv. 8 (23) (2022) eabn9231.

[26] Q. Ding, Z. Zhang, Y. Liu, K. Chai, R. Krishna, S. Zhang, One-step ethylene purification from ternary mixtures in a metal–organic framework with customized pore chemistry and shape, Angew. Chem. Int. Ed. 61 (35) (2022).

[27] Y. Wang, M. Fu, S. Zhou, H. Liu, X. Wang, W. Fan, Z. Liu, Z. Wang, D. Li, H. Hao, X. Lu, S. Hu, D. Sun, Guest-molecule-induced self-adaptive pore engineering facilitates purification of ethylene from ternary mixture, Chem 8 (12) (2022) 3263–3274.

[28] L. Yang, L. Yan, W. Niu, Y. Feng, Q. Fu, S. Zhang, Y. Zhang, L. Li, X. Gu, P. Dai, D. Liu, Q. Zheng, X. Zhao, Adsorption in reversed order of C_2 hydrocarbons on an ultramicroporous fluorinated metal-organic framework, Angew. Chem. Int. Ed. 61 (25) (2022).

[29] Y. Wang, C. Hao, W. Fan, M. Fu, X. Wang, Z. Wang, L. Zhu, Y. Li, X. Lu, F. Dai, Z. Kang, R. Wang, W. Guo, S. Hu, D. Sun, One-step ethylene purification from an acetylene/ethylene/ethane ternary mixture by cyclopentadiene cobalt-functionalized metal–organic frameworks, Angew. Chem. Int. Ed. 133 (20) (2021) 11451–11459.

[30] W. Gong, H. Cui, Y. Xie, Y. Li, X. Tang, Y. Liu, Y. Cui, B. Chen, Efficient C_2H_2/CO_2 separation in ultramicroporous metal–organic frameworks with record C_2H_2 storage density, J. Am. Chem. Soc. 143 (36) (2021) 14869–14876.

[31] C. Avci-Camur, J. Troyano, J. Perez-Carvajal, A. Legrand, D. Farrusseng, I. Imaz, D. Maspoch, Aqueous production of spherical Zr-MOF beads via continuous-flow spray-drying, Green Chem. 20 (4) (2018) 873–878.

[32] M. Fakhroleslam, S.M. Sadrameli, Thermal/catalytic cracking of hydrocarbons for the production of olefins; a state-of-the-art review III: Process modeling and simulation, Fuel 252 (2019) 553–566.

[33] M. Bonneau, C. Lavenn, J.-J. Zheng, A. Legrand, T. Ogawa, K. Sugimoto, F.-X. Coudert, R. Reau, S. Sakaki, K.-I. Otake, S. Kitagawa, Tunable acetylene sorption by flexible catenated metal–organic frameworks, Nat. Chem. 14 (7) (2022) 816–822.

[34] Y. Ye, S. Xian, H. Cui, K. Tan, L. Gong, B. Liang, T. Pham, H. Pandey, R. Krishna, P. C. Lan, K.A. Forrest, B. Space, T. Thonhauser, J. Li, S. Ma, Metal–organic framework-based hydrogen-bonding nanotrap for efficient acetylene storage and separation, J. Am. Chem. Soc. 144 (4) (2021) 1681–1689.

[35] G.-D. Wang, R. Krishna, Y.-Z. Li, W.-J. Shi, L. Hou, Y.-Y. Wang, Z. Zhu, Boosting ethane/ethylene separation by MOFs through the amino-functionalization of pores, Angew. Chem. Int. Ed. 134 (48) (2022) e202213015.

[36] W. Fan, S.B. Peh, Z. Zhang, H. Yuan, Z. Yang, Y. Wang, K. Chai, D. Sun, D. Zhao, Tetrazole-functionalized zirconium metal-organic cages for efficient C_2H_2/C_2H_4 and C_2H_2/CO_2 separations, Angew. Chem. Int. Ed. 60 (32) (2021) 17338–17343.

[37] J. Tian, Q. Chen, F. Jiang, D. Yuan, M. Hong, Optimizing acetylene sorption through induced-fit transformations in a chemically stable microporous framework, Angew. Chem. Int. Ed. 62 (7) (2023).

[38] Y. Li, X. Wang, X. Yang, H. Liu, X. Chai, Y. Wang, W. Fan, D. Sun, Fe-MOF with U-shaped channels for C_2H_2/CO_2 and C_2H_2/C_2H_4 separation, Inorg. Chem. 62 (9) (2023) 3722–3726.

[39] S. Liu, X. Li, X. Wang, Y. Li, F. Zhang, L. Li, J. Li, J. Yang, Construction of a Ti-based bimetallic metal–organic framework using a one-pot method for efficient C_2H_2/C_2H_4 and C_2H_2/CO_2 separation, Chem. Bio. Eng. 1 (5) (2024) 439–447.

[40] L.-L. Ma, N. An, F.-A. Guo, H. Wang, G.-P. Yang, Y.-Y. Wang, Separation of $C_2H_2/C_2H_4/C_2H_6$ and C_2H_2/CO_2 in a nitrogen-rich copper-based microporous metal–organic framework, Inorg. Chem. 62 (34) (2023) 13698–13701.

[41] J. Miao, W. Graham, J. Liu, E.C. Hill, L.-L. Ma, S. Ullah, H.-L. Xia, F.-A. Guo, T. Thonhauser, D.M. Proserpio, J. Li, H. Wang, An octacarboxylate-linked sodium metal–organic framework with high porosity, J. Am. Chem. Soc. 146 (1) (2023) 84–88.

[42] M.-Y. Gao, D. Sensharma, A.A. Bezrukov, Y.H. Andaloussi, S. Darwish, C. Deng, M. Vandichel, J. Zhang, M.J. Zaworotko, A robust molecular porous material for C_2H_2/CO_2 separation, Small 19 (11) (2023) 2206945.

[43] L. Wang, J. Lv, Q. Ye, Y. Luo, G.-Y. Wang, L.-H. Xie, Nanoporous Cu (II)-adenine-based metal–organic frameworks for selective adsorption of C_2H_2 from C_2H_4 and CO_2, ACS Appl. Nano Mater. 6 (23) (2023) 22095–22103.

[44] J. Wu, Y.-L. Wang, J.-P. Xue, D. Wu, J. Li, Stepwise synthesis of Cl-decorated trinuclear-Cu cluster-based frameworks for C_2H_2/C_2H_4 and C_2H_2/CO_2 separation, Inorg. Chem. 62 (49) (2023) 19997–20004.

[45] X.-Y. Zhang, W.-J. Shi, G.-D. Wang, L. Hou, Y.-Y. Wang, One Co-MOF with F active sites for separation of C_2H_2 from CO_2, $_C2_H4$, and C_H4, Inorg. Chem. 62 (40) (2023) 16574–16581.

[46] Y. Zhang, L. Yang, L. Wang, S. Duttwyler, H. Xing, A microporous metal-organic framework supramolecularly assembled from a CuII dodecaborate cluster complex for selective gas separation, Angew. Chem. Int. Ed. 131 (24) (2019) 8229–8234.

[47] X.-H. Xiong, L. Zhang, W. Wang, N.-X. Zhu, L.-Z. Qin, H.-F. Huang, L.-L. Meng, Y.-Y. Xiong, M. Barboiu, D. Fenske, H. Peng, Z.-W. Wei, Nitro-decorated microporous covalent organic framework (TpPa-NO_2) for selective separation of C_2H_4 from a $C_2H_2/C_2H_4/CO_2$ mixture and CO_2 capture, ACS Appl. Mat. Interfaces 14 (28) (2022) 32105–32111.

[48] L. Zhang, T. Xiao, X. Zeng, J. You, Z. He, C.-X. Chen, Q. Wang, A. Nafady, A.M. Al-Enizi, S. Ma, Isoreticular contraction of cage-like metal-organic frameworks with optimized pore space for enhanced C_2H_2/CO_2 and C_2H_2/C_2H_4 separations, J. Am. Chem. Soc. 146 (11) (2024) 7341–7351.

[49] Y. Han, Y. Jiang, J. Hu, L. Wang, Y. Zhang, Efficient C_2H_2/CO_2 and C_2H_2/C_2H_4 separations in a novel fluorinated metal–organic framework, Sep. Purif. Technol. 332 (2024) 125777.

[50] J. You, H. Wang, T. Xiao, X. Wu, L. Zhang, C.-Z. Lu, Introducing high concentration of hexafluorosilicate anions into an ultra-microporous MOF for highly efficient C_2H_2/CO_2 and C_2H_2/C_2H_4 separation, Chem. Eng. J. 477 (2023) 147001.